Available online at www.sciencedirect.com
SCIENCE DIRECT
Global and Planetary Change 45 (2005) 9–21
GLOBAL AND PLANETARY CHANGE
www.elsevier.com/locate/gloplacha

Hysteresis in Cenozoic Antarctic ice-sheet variations

David Pollard[a,*], Robert M. DeConto[b,1]

[a]Earth and Environmental Systems Institute, Pennsylvania State University, 2217 Earth Engineering Sciences University Park, Pennsylvania 16802-6813, USA
[b]Department of Geosciences, University of Massachusetts, Amherst, Massachusetts 01003, USA

Received 30 January 2004; accepted 28 September 2004

Abstract

A coupled global climate–Antarctic ice sheet model is run for 10 million years across the Eocene–Oligocene boundary ~34 Ma. The model simulates a rapid transition from very little ice to a large continental ice sheet, forced by a gradual decline of atmospheric CO_2 and higher-frequency orbital forcing. The structure of the transition is explained in terms of height mass balance feedback (HMBF) inherent in the intersection of the ice-sheet surface with the climatic pattern of net annual accumulation minus ablation, as found in earlier simple ice sheet models. Hysteresis effects are explored by running the model in reverse, starting with a full ice sheet and gradually increasing CO_2. The effects of higher-frequency orbital forcing on the non-linear transitions are examined in simulations with and without orbital variability. Similar effects are demonstrated with a much simpler one-dimensional ice-sheet flowline model with idealized bedrock topography and parameterized mass balance forcing. It is suggested that non-linear Antarctic ice-sheet transitions and hysteresis have played important roles in many of the observed fluctuations in marine $\delta^{18}O$ records since 34 Ma, and that the range of atmospheric CO_2 variability needed to induce these transitions in the presence of orbital forcing is ~2× to 4× pre-industrial level.

Keywords: Antarctica; Ice sheet; Cenozoic; Hysteresis; Paleoclimate

1. Introduction

Cenozoic variations of global ice-sheet volume and ocean temperatures are deduced primarily from deep-sea core records of $\delta^{18}O$ and Mg/Ca in benthic foraminifera (Zachos et al., 2001; Lear et al., 2000). These and other data suggest a long period of virtually ice-free cooling during the Eocene, until the sudden widespread glaciation of Antarctica at the Eocene–Oligocene boundary ~34 Ma. From then on, Antarctic ice volumes and/or deep-sea temperatures fluctuated significantly, with no other large ice sheets until the onset of Northern Hemispheric glaciation a few million years ago. The fluctuations since 34 Ma are

* Corresponding author. Tel.: +1 814 865 2022; fax: +1 814 865 3191.
E-mail addresses: pollard@essc.psu.edu (D. Pollard), deconto@geo.umass.edu (R.M. DeConto).
[1] Tel.: +1 413 545 3426; fax: +1 413 865 1200.

0921-8181/$ - see front matter © 2004 Elsevier B.V. All rights reserved.
doi:10.1016/j.gloplacha.2004.09.011

comprised of small-amplitude cycles on orbital timescales of 10^4 to 10^5 years, superimposed on larger fluctuations and trends with timescales of a few hundred thousand to several million years (Zachos et al., 2001).

Modeling studies have shown that ice sheets can respond non-linearly as climate varies, with sudden transitions in ice-sheet size between multiple stable branches. This hysteresis is a straightforward geometric consequence of the intersection of the ice-sheet surface with typical spatial patterns of net annual snowfall minus ablation, and does not involve albedo feedback (Weertman, 1961, 1976; Oerlemans and van der Veen, 1984; Oerlemans, 1981, 1982a, 2002a). There are two types of hysteresis effects. One, shown in Fig. 1a, involves the formation of relatively small ice caps on sloping terrain, where ice caps below a certain finite size are unstable (analogous to Weertman, 1976, his Fig. 3).

The other type of hysteresis applies to continental ice sheets bounded by the ocean, such as East Antarctica (Fig. 1b, after Oerlemans, 2002a). Starting with no ice and a warm climate, temperatures must cool considerably before any ice appears, since the annual snowline must descend all the way to the ice-free surface. The non-linearity is most pronounced with no topography and a flat snowline, as in Fig. 1b. In this case, ice grows suddenly over the entire surface, forming a full continental ice sheet with positive mass balance everywhere, discharging into the ocean. If the climate then becomes gradually warmer, the snowline must ascend considerably to produce appreciable melt on the outer ice-sheet flanks, which rise steeply into colder air from the coast and occupy relatively little horizontal area. At first, this outer melt is balanced by dynamical ice flow from the interior and no marginal retreat occurs. The ice sheet will only start to retreat when the areally averaged ice-sheet mass balance is

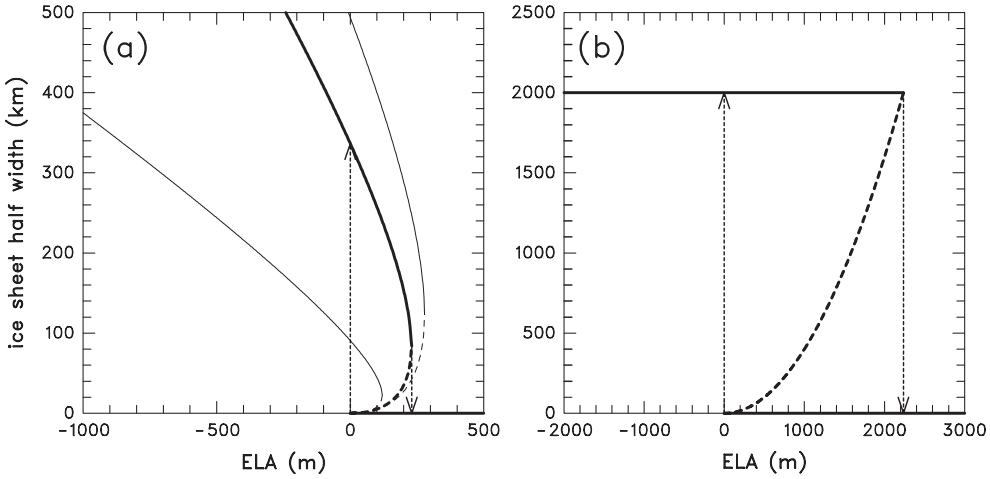

Fig. 1. Equilibrium ice-sheet sizes versus climate forcing in simple one-dimensional plastic models forced by prescribed patterns of surface mass balance. Thick solid lines indicate stable solutions, thick dashed lines indicate unstable solutions and dotted arrows indicate possible transitions. The solutions are dimensional (not normalized) in order to relate the magnitudes to Antarctica. In all cases, the slope of the snowline or terrain is zero or 0.003, appropriate for major Antarctic mountain ranges. The net surface mass balance has uniform values above and below the snowline, with the value below (negative) being 3× that above (positive). The plastic rheological constant (λ in Appendix A) is 10 m. (a) Flat snowline and sloping terrain away from a central peak, appropriate for an isolated mountain range (as in Fig. A1; see Appendix A for analysis). ELA is the elevation of the snowline above the central peak. The upper thinner solid and dashed lines are for a loosely analogous case, with flat terrain and a snowline sloping upwards in both directions from a central minimum. ELA is the elevation of the central snowline minimum above the land. The analysis for this case parallels that in Weertman (1976), the only difference being the form of the normalization factors. The lower thinner lines show Weertman's (1976, his Fig. 3) case for comparison, with flat terrain bounded on the poleward side and a sloping snowline, and requiring zero net mass balance for the southern half only (more appropriate for Northern Hemispheric ice sheets). ELA is the snowline elevation above land at the poleward boundary. (b) Flat snowline on a flat bounded continent of width 4000 km (after Oerlemans, 2002a, Fig. 1). ELA is the elevation of the snowline above the land. Unlike the cases in (a), non-zero stable solutions have positive net mass balance, discharging to the continental shorelines. Note the much larger axes values in (b) compared to (a); the ice-sheet sizes and magnitude of hysteresis in (b) are much larger.

negative, i.e., when the snowline has risen far above the original bedrock surface, much higher than the elevation needed to grow the ice sheet originally. At that point, the positive feedback of more melt with lowering ice surface (height mass balance feedback, HMBF) produces runaway wastage of the ice sheet, returning to a state of no ice. Related studies show that hysteresis of either type may also be important for Greenland (Abe-Ouchi and Blatter, 1993; Crowley and Baum, 1995; Toniazzo et al., 2004) and the Laurentide (Weertman, 1976; Birchfield, 1977; Pollard, 1978).

These concepts have been investigated in the context of Cenozoic Antarctic variations by Oerlemans (1982b) and Huybrechts (1993, 1994), using 3-D ice sheet models and prescribed climate variations. Huybrechts found ice-volume hysteresis in experiments with a cooling climate starting with no ice, versus warming climates starting with full ice; however, the amount of hysteresis was quite small, with only ~1 °C difference in air temperature between the growing and receding branches (or ~4 °C with no bedrock topography). He also found that the climate regime in which transitions occur is ~10 to 20 °C warmer than present; i.e., the present Antarctic climate would have to warm into that range to cause drastic retreat or collapse of the current East Antarctic Ice Sheet (EAIS).

The main purpose of this paper is to extend these investigations to include orbital variability and predicted climates, using a coupled 3-D ice sheet and global climate model (GCM) as in DeConto and Pollard (2003a,b), in order to assess the importance of hysteresis in Antarctic ice-sheet fluctuations through the Cenozoic. A related examination of Cenozoic Antarctic ice volumes has recently been performed by Oerlemans (2004, in press) using a simple 1-D plastic ice sheet model, not focusing on hysteresis effects but rather on distinguishing between ice volume and deep-sea temperature signals. Most other modeling studies of Cenozoic Antarctic ice-sheet variations have considered relatively small changes from the present, such as the effects of warming in the next few hundred years (e.g., [Huybrechts and Oerlemans, 1990; Huybrechts and de Wolde, 1999), and Quaternary variability (Huybrechts, 1990a,b; Ritz et al., 2001; Oerlemans, 2002b).

The climate–ice sheet coupling used in this paper captures HMBF as ice-sheet surface elevations vary, which is crucial for the non-linear hysteresis effects described above. As explained in Section 2, however, the albedo feedback of ice-sheet extent on the climate is only roughly captured, and not at all for sudden transitions. Previous modeling studies have shown that ice-albedo feedback can produce "Small Ice Cap Instability" (SICI), i.e., non-linear jumps and hysteresis in energy-balance climate models (EBMs) that resemble those of HMBF, despite the entirely different physical mechanisms involved (e.g., North, 1975, 1984; Birchfield et al., 1982; Mengel et al., 1988). The ice-albedo/SICI mechanism has been investigated for Antarctica using EBMs and GCMs by Crowley et al. (1994) and indirectly by Ogura and Abe-Ouchi (2001), and using a coupled EBM–ice sheet model by Maqueda et al. (1998). Since the effects of ice-albedo feedback and HMBF are similar and have the same sign, they would be expected to augment and increase the hysteresis effects described below. The discussion above applies to the albedo feedback (and other climatic effects) of the *terrestrial* ice sheet; in our model, seasonal albedo feedback of sea ice and snow are fully captured by the GCM.

It should be noted that the model described below, and most of those mentioned above, are limited to the terrestrial EAIS. Possible marine incursions and instability of the West Antarctic Ice Sheet (WAIS) (e.g., Hughes, 1975; Warner and Budd, 1998; Anderson et al., 2001; Vaughan and Spouge, 2002), presently grounded well below sea level, are not represented. The WAIS may not have existed in the earlier Cenozoic (Scherer, 1991), and later WAIS fluctuations have arguably occurred with higher frequencies and smaller amplitudes than those considered here (Pollard, 1983, Appendix; MacAyeal, 1992; Oerlemans, 2002b).

2. Models and coupling methods

The experiments in this paper use a coupled GCM–dynamic ice sheet model, and focus on the Eocene–Oligocene transition ~34 Ma. The models, boundary conditions and coupling are described in DeConto and Pollard (2003a,b) and Pollard and DeConto (2003). Briefly, the GENESIS v.2 global climate model (Thompson and Pollard, 1997) is run with T31 horizontal resolution (~3.75°) and a 50-m slab ocean to simulate a suite of climates for the Cenozoic, with

prescribed orbital configurations representing idealized orbital cycles. The stored monthly climate fields are interpolated to the fine-grid (40 km) topography of the Antarctic ice sheet model, using constant lapse-rate corrections as in Thompson and Pollard (1997).

A positive-degree day parameterization is used to calculate the net annual surface mass balance in the ice sheet model (e.g., Ritz et al., 1997) every 200 years as the ice topography varies, with allowance for diurnal cycles, superimposed ice and refreezing of meltwater. A standard 3-D dynamic ice sheet model is used, following the established lineage of Huybrechts (1990a), Ritz et al. (1997) and others. The ice model is run on a 40-km polar stereographic grid, with 10 vertical levels and a timestep of 10 to 20 years. Ice temperatures are predicted mainly for their effects on ice rheology and basal conditions. Vertical diffusive temperature profiles are also predicted through the upper ~2 km of bedrock, using six unequal levels, and a uniform geothermal heat flux. Standard basal sliding occurs where the bed is at the melting point; there is no other consideration of basal hydrology or deforming beds. There are no ice shelves, and ice is removed seaward of the continental shoreline (thus, the initiation of West Antarctic ice, which requires a phase of expanding ice shelves or calving fronts, is postponed to future work). The bedrock response to ice load is a local relaxation to isostatic equilibrium with a time constant of 5000 years, and with the load modified by lithospheric flexure (Brotchie and Sylvester, 1969). The GCM Cenozoic simulations use a reconstruction of early Oligocene geography, topography and sea level (Hay et al., 1999). The higher-resolution ice sheet model uses present-day Antarctic bedrock elevations (Bamber and Bindschadler, 1997), isostatically rebounded with present ice removed.

Since it is computationally infeasible to run the GCM continuously over geologic time scales, the coupling between the climate and ice sheet models is necessarily asynchronous. First, a suite of five GCM climate simulations is performed, with orbital configurations updated every 10,000 years in order to resolve an idealized orbital cycle with 20, 40 and 80 ka periodicities (explained in detail in DeConto and Pollard, 2003a,b). In-between each GCM simulation, the ice sheet model is run for 10,000 years driven by the previous GCM climate, and the resulting ice extent is prescribed for the next GCM simulation. Two such GCM suites are generated with different atmospheric CO_2 levels, 2× and 3× PAL (pre-industrial atmospheric level, taken as 280 ppmv). Subsequently, the stored suites of monthly meteorologic GCM variables are averaged appropriately to provide the climate and surface mass balance at any time as the ice sheet model is integrated continuously through millions of years. The averaging of the GCM climates (temperature, precipitation) is linear, accounting for orbital cycles and imposed long-term trends in CO_2. For CO_2, the interpolation is performed in terms of $\log(CO_2)$ to account for its logarithmic effect on radiative forcing; for values outside the range of 2× to 3× PAL, linear extrapolation is performed. Although this procedure roughly captures some albedo feedback due to higher-frequency ice-sheet and sea-ice variability in response to orbital cycles, in general, it does not account for ice-albedo feedback in the long-term simulations. This is especially true across major ice transitions such as the Eocene–Oligocene boundary, where the ice-sheet expansion in the long-term simulation does not correspond at all to the ice sheets in the GCM sequences. However, since varying ice-sheet topography is accounted for in the surface mass balance computations every 200 years, height mass balance feedback is captured adequately.

3. Results: ice volume

The solid curve in Fig. 2a shows Antarctic ice volume from a 10-million-year simulation representing the Eocene–Oligocene transition (DeConto and Pollard, 2003a,b), with imposed orbital forcing and a long term linear decline in atmospheric CO_2 from 4× to 2× PAL over the duration of the run. This CO_2 history around the E–O boundary is more or less consistent with estimates from geochemical models (Berner and Kothavala, 2001) and deep-sea core data (Pagani et al., 1999; Pearson and Palmer, 2000; but see Royer et al., 2001; Demicco et al., 2003). As discussed in DeConto and Pollard (2003a,b), the relatively sudden non-linear transition from very small ice amounts to a near continental expanse as CO_2 drops slightly below 3× PAL, and the higher-frequency orbital variations, bear a striking resemblance to the observed Eocene–Oligocene transition in $\delta^{18}O$ records (Zachos et al., 1996, 2001).

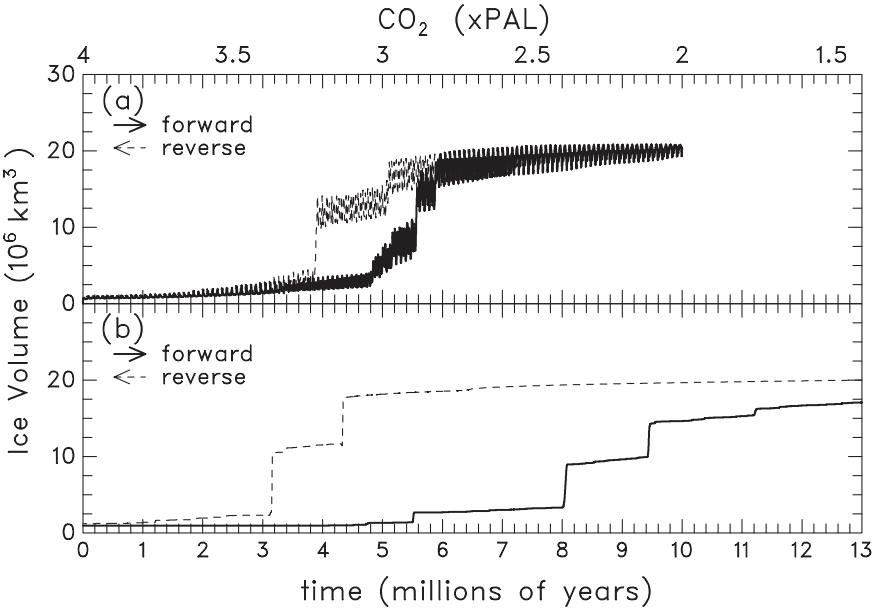

Fig. 2. Antarctic ice volumes in ~10-million-year simulations with the ice sheet model driven asynchronously by stored GCM climates. (a) Solid curve: "forward" integration, running from left to right with atmospheric CO_2 decreasing linearly in time from 4× to 2× PAL, and with higher-frequency orbital forcing. Dashed curve: "reverse" integration, running from right to left, starting with a large ice sheet, and with CO_2 increasing linearly from 2× to 4× PAL. (b) As (a), except with no orbital forcing.

We interpret the overall transition as a bounded-continent jump of the second type mentioned in the Introduction, as the snowline descends below the level of most Antarctic terrain and the ultimate size is constrained only by the shoreline (as in Fig. 1b). The overall transition is made up of three smaller "substeps", which occur as the descending snowline intersects the plateaus of the major mountain ranges (Queen Maud, Gamburtsevs, Transantarctics), allowing substantial ice caps to form on each, which then fluctuate with orbital forcing and later coalesce. One might consider these substeps to be jumps of the first type mentioned above involving sloping terrain; however, for slope magnitudes appropriate for the Antarctic ranges, this mechanism produces very little hysteresis (only very small initial ice caps ~100 km wide, as in Fig. 1a) and quite gradual subsequent growth, unlike the model substeps in Fig. 2a. Hence, we think the substeps are more likely manifestations of the continental-scale mechanism (Fig. 1b), occurring as the snowline intersects the more or less flat central plateau of each mountain range, with the ice cap bounded for a while by the extent of the range. More analysis on the scale of mountain ranges is given in Oerlemans (2002a). Fig. 3 further illustrates the model behavior, showing baseline (ice-free) bedrock topography, and snapshots of ice thickness through the transition.

The dashed curve in Fig. 2a shows a reversed run, starting with a full continental ice sheet under a warming climate, i.e., with time running from right to left and CO_2 linearly *increasing* from 2× to 4× PAL. As expected from the continental ice-sheet hysteresis found in simple models as described above (Fig. 1b), the main transition is delayed compared to the forward simulation. This is simply because the pre-existing ice-sheet topography is much higher and steeper than the baseline bedrock topography, so the snowline has to be raised substantially before the overall ice-sheet budget becomes negative. The same minor substeps occur as in the forward integration, as ice retreats from individual mountain plateaus.

The lower panel in Fig. 2b shows the same pair of forward and reversed runs, but with no orbital cycles, i.e., with the same mid-range orbit throughout, and the slow CO_2 trend as the only external forcing. Without orbital variability, the main transition and the substeps are delayed considerably, and the hysteresis between

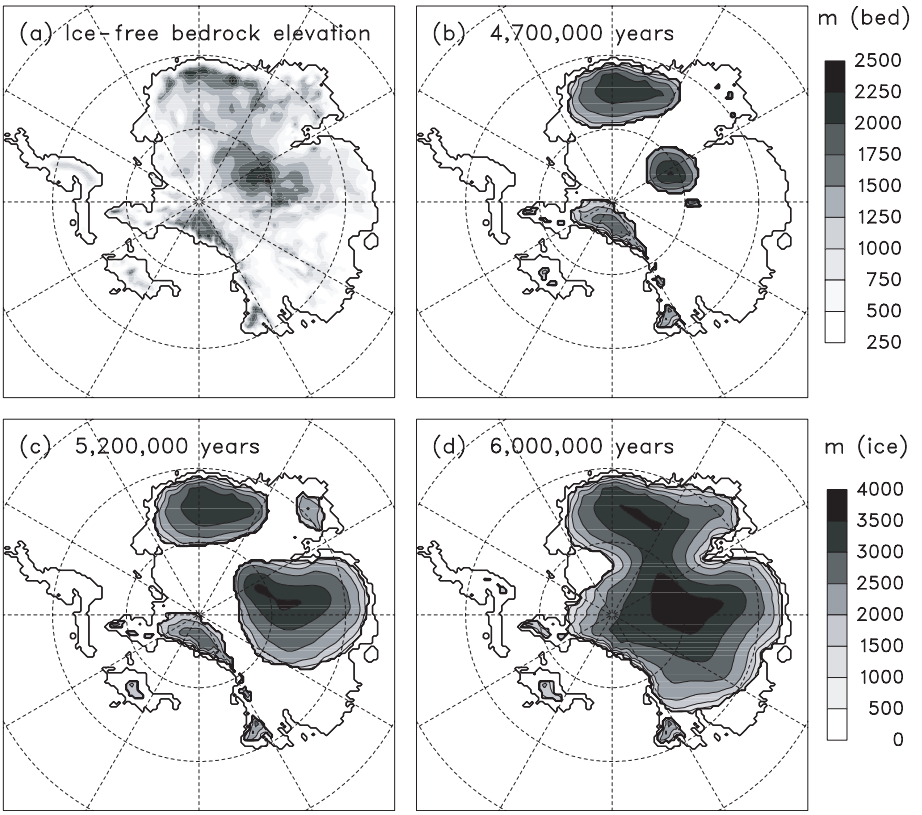

Fig. 3. (a) Ice-free Antarctic bedrock topography in meters above sea level, reconstructed from a modern 5-km database (Bamber and Bindschadler, 1997), isostatically relaxed to ice-free equilibrium and interpolated to the 40-km polar stereographic grid of the ice sheet model. (b–d) Ice surface elevations at particular times during the major transition from little ice to a large continental ice sheet in the nominal long-term simulation (Fig. 2a, solid curve). (b) 4,700,000 years. (c) 5,200,000 years. (d) 6,000,000 years. These are model years from the start of the long integration, as shown on the horizontal axis in Fig. 2.

forward and reversed runs increases several fold. Evidently, orbital cycles act as an "envelope" of high-frequency forcing superimposed on the gradual CO_2 trend, so that particular thresholds are reached earlier than in the absence of orbital forcing. For instance, when the descending snowline in the forward run in Fig. 2b is still above a mountain plateau, an austral-summer cold orbit can lower the snowline in Fig. 2a to intersect the plateau, growing a substantial ice cap in a few thousand years that can survive the next austral-summer warm orbital interval. In other words, without high-frequency orbital variability, the CO_2 trend must continue for longer to achieve a particular snowline-elevation threshold.

Much the same behavior is exhibited by simpler models with idealized forcing, as shown in Fig. 4. Here, the ice sheet model has been reduced to a single one-dimensional Cartesian flowline, with no lithospheric flexure and no ice-temperature variation. The continental domain is 3000 km wide with zero ice imposed at each boundary. The ice-free bedrock topography is 0 m, except for two triangular "mountain ranges" equi-spaced on the domain with width 700 km and central peak elevation 2000 m. The surface mass balance is parameterized in terms of the Equilibrium Line Altitude (ELA), whose elevation is flat but varies in time. For an ice surface at Z meters above sea level, the net annual mass balance B (m/year) is:

$$B = \max\left[.05, \mathrm{e}^{-Z/1000}\right] \quad \text{if } Z>\mathrm{ELA}$$

$$B = (\mathrm{ELA} - Z)/1000 \quad \text{if } Z<\mathrm{ELA}$$

which crudely captures the elevation-desert reduction in snowfall in the high Antarctic interior, and rapid

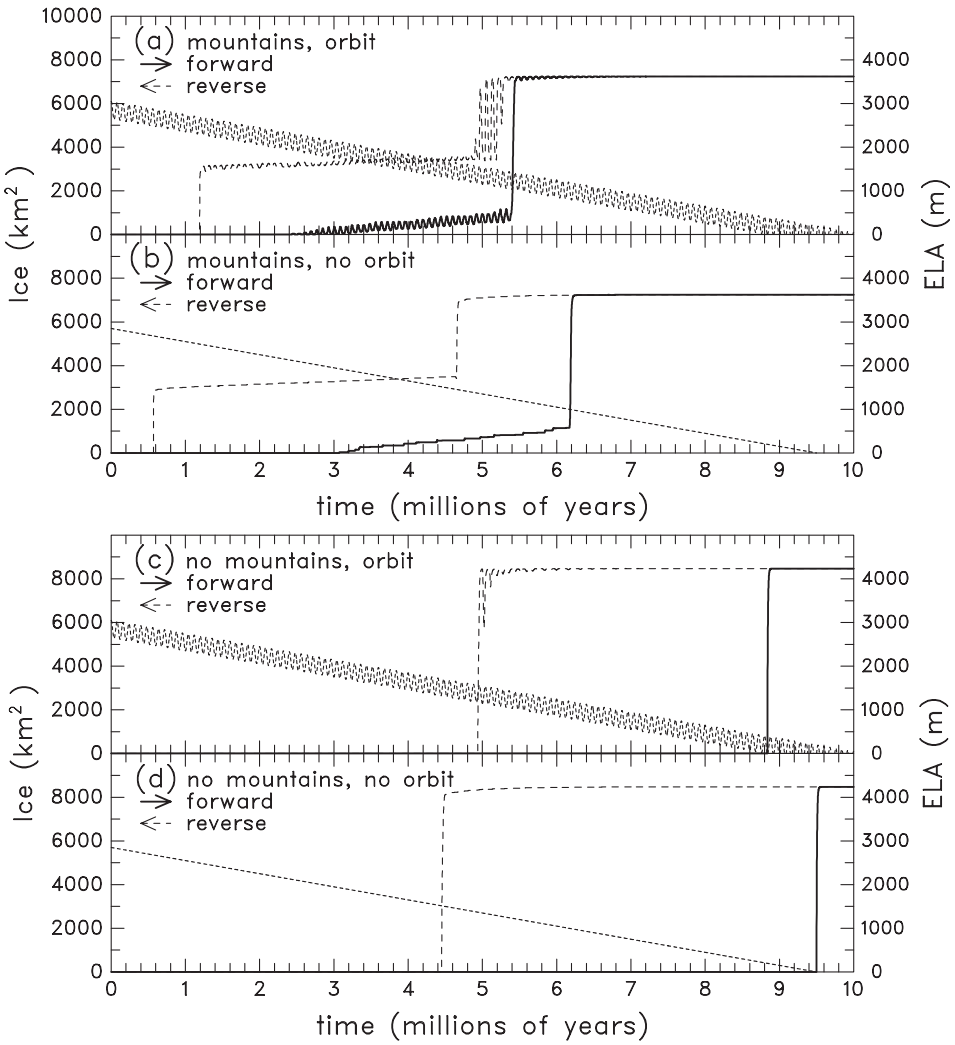

Fig. 4. As Fig. 2, except showing ice-sheet cross sectional area, using a 1-D flowline ice model, idealized baseline bedrock topography, and parameterized surface mass balance (see text). The fine-dashed lines and right-hand scale show prescribed variations in Equilibrium Line Altitude (ELA, see text). (a) With orbital forcing and mountain ranges. (b) With no orbital forcing, and with mountain ranges. (c) With orbital forcing and no mountains (flat baseline topography). (d) With no orbital forcing and no mountains.

increase in melting below the ELA. Long-term forcing is imposed by lowering or raising the ELA by 300 m per million years (fine-dashed lines and right-hand scale in Fig. 4). Orbital forcing is imposed as an additional sinusoidal variation with a peak-to-peak amplitude of 400 m and a period of 80 ka.

All of the non-linear features in the full-model runs (Fig. 2) have their counterparts in Fig. 4. With orbital forcing and mountains (Fig. 4a), there is a substep within the overall transition as ice caps first form on (retreat from) the mountains in the forward (reverse) run. With no orbital forcing (Fig. 4b), the hysteresis is more pronounced, and transitions are delayed on the order 200/300 million years, which is the time needed by the long-term CO_2 trend to raise or lower the ELA by 1/2 the amplitude of the orbital forcing.

Fig. 4c and d shows the effects of removing the two mountain ranges, so that the ice-free bedrock elevation is 0 m everywhere. There are no substeps in this case, and all hysteresis is due to the continental-scale

mechanism of the flat snowline intersecting the flat baseline bedrock in the forward direction, and having to counteract the ice-sheet topography in the reverse direction. Compared to the runs with mountains, the transitions occur later and more abruptly, and hysteresis is more pronounced, as might be expected without the substeps provided by mountain plateaus.

4. Results: temperature and precipitation

Fig. 5 gives an idea of the relative effects of orbital changes and CO_2 variations on the GCM climate, showing changes in austral summer surface air temperature and annual precipitation over Antarctica with a prescribed large Antarctic ice sheet like that in Fig. 3d. Since ice melt occurs only in the summer months and only on the lower-elevation flanks (~70 S), summer air temperatures in those regions are most relevant to the annual ice-sheet mass balance. Around the flanks, extreme orbital changes produce 4 to 8 °C of summer warming, comparable to the 4 to 6 °C warming produced by increasing CO_2 from 2× to 3× PAL. Orbitally induced warming in the interior (Fig. 5a) is even greater, but this has no direct effect on the ice budget. Precipitation increases along with temperature over the whole region with both types of forcing (Fig. 5c,d), due primarily to the greater moisture capacity of warmer air, with larger increases in absolute amount around the lower flanks and surrounding ocean.

The 4 to 6 °C flank warming due to increased CO_2 (Fig. 5b) gives a rough estimate of the temperature

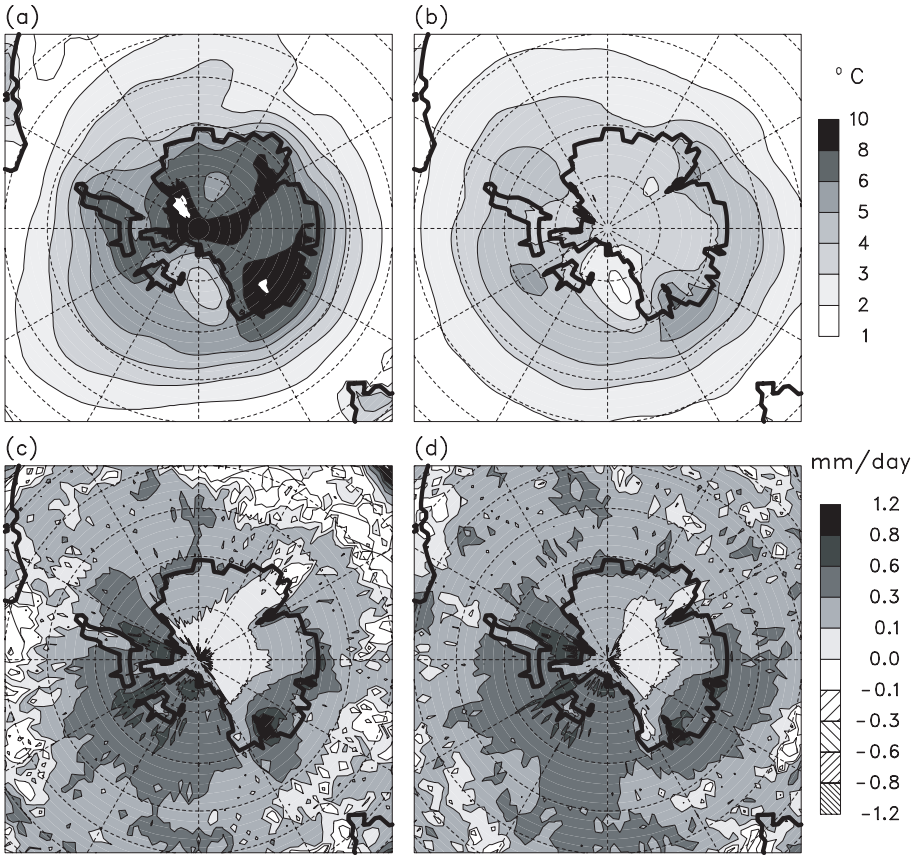

Fig. 5. (a) Difference in austral summer (DJF) 2-m air temperature (°C) with a full ice sheet, between two GCM simulations with orbits yielding extreme warm minus extreme cold Southern Hemispheric summers (Warm orbit has eccentricity 0.05, perihelion in January, obliquity 24.5°. Cold orbit has eccentricity 0.05, perihelion in July, obliquity 22.5°). (b) As (a), except for 3× minus 2× PAL CO_2, both with the cold SH summer orbit. (c–d) As (a) and (b), except for changes in annual precipitation (mm/day).

difference associated with the hysteresis in Fig. 2. With orbital forcing, the forward and reverse transitions in Fig. 2a are separated by 0.5× PAL in CO_2 amount (~2.7× vs. 3.2×), i.e., by ~2 to 3 °C in summer temperatures around ~70 °S judging from Fig. 5b. Without orbital forcing, the hysteresis separation in Fig. 2b is ~1× PAL (~2× vs. 3×), i.e., ~4 to 6 °C in summer temperatures around ~70 °S. The latter temperature difference is larger than the ~1 °C separation found in Huybrecht's Antarctic simulations (Huybrechts, 1993, his Fig. 9). Presumably, this is due to differences in climate variations, since the ice sheet models and baseline topography are very similar in both studies. For instance, increases in GCM snowfall (Fig. 5c,d) tend to counteract the increases in flank temperatures and melt, possibly to a greater extent than in the surface mass-balance parameterizations of Huybrechts (1993,1994).

Fig. 6 summarizes the sensitivity of GCM surface air temperatures and precipitation to a more complete set of changes in CO_2, orbit, and ice-sheet size. Temperatures in Fig. 6a are for austral summer, averaged around 65 °S (just offshore to avoid topographic effects of different ice-sheet geometries). With no ice, the effects of an extreme orbital change are somewhat larger than a 2× to 3× CO_2 change. With full ice, the effects are comparable (as in Fig. 5), and are largest for the coldest conditions where there is more opportunity for sea-ice-albedo feedback.

Changes in annual precipitation shown in Fig. 6b closely follow those of temperature (due primarily to the greater moisture capacity of warmer air) and have opposite effects on the ice-sheet mass balance. The effects of melt on the overall mass balance generally dominate those of precipitation, for the large excursions considered here (as evident in Fig. 2, unlike the smaller changes from the colder modern base state expected in the next century; e.g., [Huybrechts and Oerlemans, 1990; Huybrechts and de Wolde, 1999]). Not shown in Fig. 6 are the very different *spatial* distributions of precipitation for a full ice sheet compared to no ice, with strong orographic precipitation on ice-sheet flanks and desert-like conditions in the interior; the interior-desert and cooling effects of a full ice sheet dominate those of orography to lower the continental-mean precipitation (Fig. 6b).

Fig. 6 also shows values from a modern GCM simulation with the present Antarctic ice sheet (Thompson and Pollard, 1997). Compared to modern, summer flank temperatures are ~10 °C warmer with 3× PAL CO_2 (Fig. 6a), which is roughly the CO_2 value at which the main reverse transition occurs in Fig. 2b.

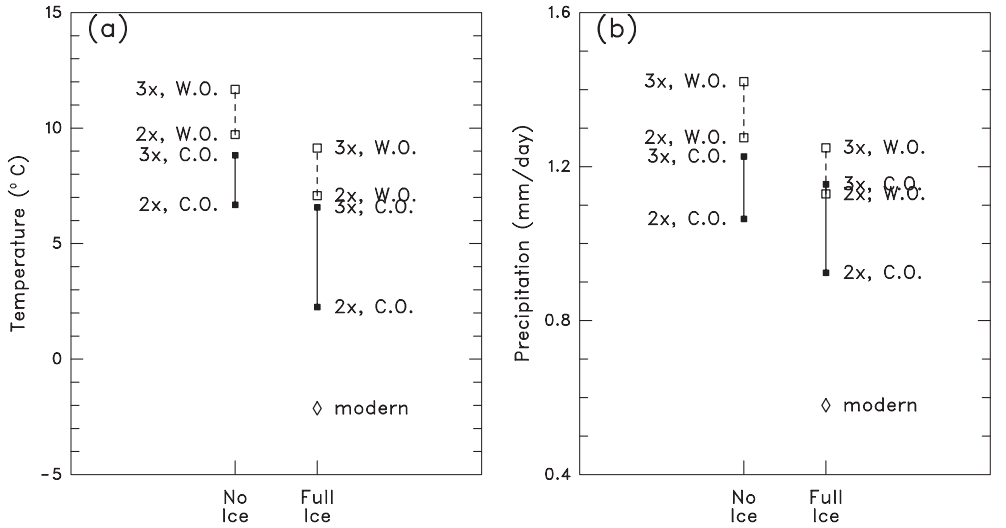

Fig. 6. (a) Austral summer (DJF) 2-m air temperatures averaged around the 65 °S latitude circle, for various GCM climates with two prescribed orbits (C.O. and W.O. denote austral-summer cold and warm orbits as in Fig. 5), two CO_2 levels (2× and 3× PAL), and two prescribed ice-sheet extents (no ice, and a "full" continental ice sheet as at the end of the forward run in Fig. 2a). Also shown is the value for a modern simulation with the present Antarctic ice sheet. (b) As (a), except for annual mean precipitation, averaged over the Antarctic continent.

This is somewhat less than the ~15 to 20 °C warming above modern required to cause EAIS retreat found by Huybrechts (1993, his Fig. 9). Again, this may reflect differences in the treatment of precipitation between the two studies, but is probably due more to shortcomings of our coupling method in Fig. 2 (see below).

5. Conclusions

Non-linear transitions and hysteresis associated with ice-sheet height mass balance feedbacks are likely to be important in Cenozoic variations of Antarctic ice volume. In our coupled climate–ice sheet model, the observed sudden onset of Antarctic ice at the Eocene–Oligocene boundary ~34 Ma is simulated successfully as a non-linear response triggered by gradual decline of atmospheric CO_2, with height mass balance feedbacks being central to the suddenness of the transition. The transitions and hysteresis in our results are interpreted as due to the continental-scale mechanism of a flat snowline and bounded ice extent (Fig. 1b). As discussed in DeConto and Pollard (2003a), other influences such as the opening of the Drake and Tasman Passages and changing ocean circulation are probably minor in comparison. We suggest that the same type of non-linear responses of the Antarctic ice sheet have played important roles in many of the subsequent 10^5- to 10^6-year fluctuations in the composite $\delta^{18}O$ record since 34 Ma (Zachos et al., 2001).

In our model with orbital forcing, CO_2 levels need to rise slightly above 3× PAL to induce drastic retreat of a pre-existing EAIS, and need to drop slightly below 3× PAL to grow a large ice sheet from no ice (Fig. 2a). However, our current coupling method does not fully capture terrestrial ice–albedo feedback, which can affect Antarctic temperatures and precipitation just as much as orbital and CO_2 changes, as shown by Fig. 6. Work is in progress to incorporate this effect. In preliminary experiments including orbital forcing (not shown), we have found that albedo feedback increases the hysteresis between forward and reverse runs, so that transitions occur at 3× and 4× PAL CO_2, and are more sudden than those in Fig. 2a.

These results have significant implications for the possible envelope of East Antarctic ice-sheet behavior through the Cenozoic. Once a large EAIS forms at the Eocene–Oligocene transition, then in order for any subsequent large-scale retreat of the ice sheet to occur, the decline in atmospheric CO_2 must reverse and levels must rise above ~3 to 4× PAL in the presence of orbital forcing. As mentioned above, Huybrechts (1993, 1994) has addressed much the same question regarding Cenozoic Antarctic ice-sheet variability, using a similar ice model to ours with parameterized climate forcing. Our results suggest that if CO_2 levels fluctuated between ~2× and 4× PAL through the Oligocene, Miocene and/or Pliocene, this would have produced the right range of high-southern-latitude climates to trigger repeated non-linear jumps and hysteresis in Antarctic ice volume. This CO_2 range is somewhat higher than the ~1× to 1.5× PAL deduced from proxy records between 25 Ma and the present (Pagani et al., 1999; Pearson and Palmer, 2000; Zachos et al., 2001; Royer et al., 2001; Demicco et al., 2003), but arguably still plausible given the uncertainties in those estimates (cf. Retallack, 2001, 2002).

Due to the mass inertia of the ice sheet, climate fluctuations out of equilibrium with current ice must be maintained for several thousand years to have an appreciable effect on East Antarctic ice volume, and to induce transitions such as those described above. Some higher-end projections of long-term anthropogenic CO_2 levels exceed ~3× to 4× PAL for several thousand years into the future (Walker and Kasting, 1992; Lenton and Cannell, 2002), which are the levels needed in our model to induce EAIS collapse. However, our paleoclimatic simulations are not directly applicable to the next ~5000 years, since the time scales of CO_2 change are very different, and since we include full orbital variations. Also, the no-orbit case in Fig. 2b does not include the albedo-cooling effect of a full-size Antarctic ice sheet. In preliminary experiments with albedo feedback and no orbital variations, we find that CO_2 levels must exceed ~8× PAL to induce significant retreat from full ice-sheet conditions, more in line with Huybrechts'(1993) finding that 15 to 20 °C local warming is necessary to induce drastic retreat of the modern EAIS.

Acknowledgements

We thank Ayako Abe-Ouchi and Robert Oglesby for careful and helpful reviews. This work was funded

by the U.S. National Science Foundation under collaborative grant ATM-9905890/9906663.

Appendix A. Plastic ice sheet on sloping terrain

We considered the idealized geometry shown in Fig. A1 as a possible analogy for the substeps in Fig. 2a, as individual ice caps form and decay on the mountain ranges of Antarctica. As explained in the text, its stability results (Fig. 1a) turned out to be not very relevant to our main model behavior. However, the analysis of this case may be of interest for its own sake, and is presented below. A more heuristic approximate solution is used by Oerlemans (2003).

For a given ice-sheet size L (half-width from the central peak to the ice edge), we need to derive the ice surface profile. The elevation of the ice-sheet surface h versus horizontal distance from the central peak x obeys:

$$(h + sx)\frac{\partial h}{\partial x} = -\frac{\lambda}{2} \tag{A1}$$

where s is the slope (positive downwards) of the undisturbed bedrock away from the peak, and $\lambda=(2\tau/\rho_i g)(1-\rho_i/\rho_b)$. Here, τ is the constant plastic basal shear stress, g is the gravitational acceleration, and ρ_i and ρ_b are densities of ice and bedrock, respectively. All elevations including h are relative to the undisturbed bedrock peak. Eq. (A1) and λ follow from the usual shallow-ice and plastic approximations and isostatic depression of bedrock.

We were unable to find an analytic solution $h(x)$ of Eq. (A1). But by switching dependent and independent variables h and x and re-arranging, Eq. (A1) becomes:

$$\frac{\partial x}{\partial h} + \frac{2s}{\lambda}x = -\frac{2}{\lambda}h \tag{A2}$$

which is solvable analytically for x as a function of h, with the boundary condition that $x=L$ at $h=-sL$. The solution is:

$$x = \frac{\lambda}{2s^2}\left[1 - e^{-\frac{2s}{\lambda}(h+sL)}\right] - \frac{h}{s} \tag{A3}$$

This is valid for x between 0 and L, i.e., for h between the central ice elevation h_c and $-sL$. The value of h_c may be found by a numerical search (e.g., Newton–Raphson iteration) yielding the zero of the right-hand side of Eq. (A3).

The switch of variables from $h(x)$ to $x(h)$ is convenient in finding the net mass balance of the ice sheet for a given flat snowline elevation E, with uniform accumulation rate a above and uniform ablation rate a' below. The distance from the center to the intersection of the snowline and ice surface, x_e say, is given immediately by the right-hand side of Eq. (A3) with h replaced by E (if E is between $-sL$ and h_c). The average mass balance for the whole ice sheet is $a(x_e/L)-a'(1-x_e/L)$. Thus, a 2-D map of ice mass balance versus L and E can quickly be computed numerically with very fine increments of L and E, whose zero-contours are the thick solid and dashed curves in Fig. 1a.

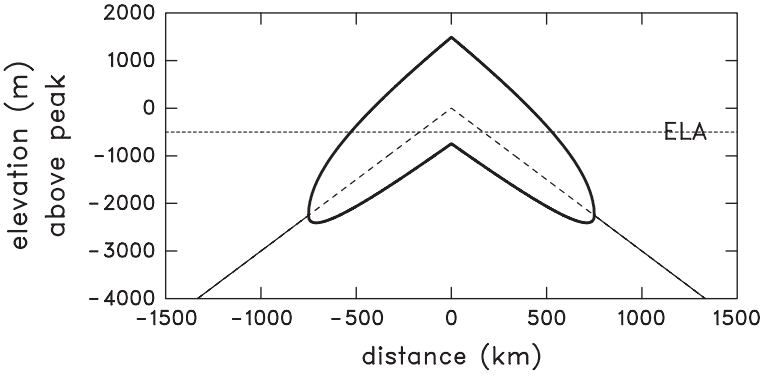

Fig. A1. Geometry of a 1-D plastic ice sheet on sloping terrain with a central peak (unbounded triangular mountain range). Thick solid lines show the ice surface and bed, thin solid and dashed lines show undisturbed bedrock elevation, and the flat dotted line shows the snowline (ELA).

Although not needed here, the total ice-sheet volume V (actually cross-sectional area) for a given L is:

$$V = 2\left(\int_{-sL}^{h_c} x(h)\mathrm{d}h - \frac{sL^2}{2} \right) \frac{1}{(1-\rho_i/\rho_b)} \qquad \text{(A4)}$$

where the integral is an algebraic expression derived straightforwardly from Eq. (A3), the term $-sL^2/2$ removes the solid-earth triangular area as if there was no bedrock depression, and $1/(1-\rho_i/\rho_b)$ allows for isostatic depression. The central ice elevation h_c must be found from Eq. (A3) as above by Newton–Raphson (or other) iteration.

References

Abe-Ouchi, A., Blatter, H., 1993. On the initiation of ice sheets. Ann. Glaciol. 18, 203–207.

Anderson, J.B., Smith Wellner, J., Lowe, A.L., Mosola, A.B., Shipp, S.S., 2001. Footprint of the expanded West Antarctic Ice Sheet: ice stream history and behavior. GSA Today, Geol. Soc. Am. 11 (10), 4–9.

Bamber, J.A., Bindschadler, R.A., 1997. An improved elevation dataset for climate and ice-sheet modeling: validation with satellite imagery. Ann. Glaciol. 25, 439–444.

Berner, R.A., Kothavala, Z., 2001. GEOCARB III: a revised model of atmospheric CO_2 over Phanerozoic time. Am. J. Sci. 301, 182–204.

Birchfield, G.E., 1977. A study of the stability of a model continental ice sheet subject to periodic variations in heat input. J. Geophys. Res. 82, 4909–4913.

Birchfield, G.E., Weertman, J., Lunde, A.T., 1982. A model study of the role of high-latitude topography in the climatic response to orbital insolation anomalies. J. Atmos. Sci. 39, 71–87.

Brotchie, J.F., Sylvester, R., 1969. On crustal flexure. J. Geophys. Res. 74, 5240–5252.

Crowley, T.J., Baum, S.K., 1995. Is the Greenland ice sheet bistable? Palaeoceanography 10, 357–363.

Crowley, T.J., Yip, K.-J., Baum, S.K., 1994. Snowline instability in a general circulation climate model; application to Carboniferous glaciation. Clim. Dyn. 10, 363–376.

DeConto, R.D., Pollard, D., 2003a. Rapid Cenozoic glaciation of Antarctica triggered by declining atmospheric CO_2. Nature 421, 245–249.

DeConto, R.D., Pollard, D., 2003b. A coupled climate-ice sheet modeling approach to the early Cenozoic history of the Antarctic ice sheet. Palaeogeogr. Palaeoclimatol. Palaeoecol. 198, 39–52.

Demicco, R., Lowenstein, T.K., Hardie, L.A., 2003. Atmospheric pCO_2 since 60 Ma from records of seawater pH, calcium and primary carbonate mineralogy. Geology 31, 793–796.

Hay, W.W., DeConto, R.M., Wold, C.N., Wilson, K.M., Voight, S., Schulz, M., Wold-Rossby, A., Dullo, W.-C., Ronov, A.B., Balukhovsky, A.N., 1999. An alternative global Cretaceous paleogeography. In: Barrera, E., Johnson, C. (Eds.), The Evolution of Cretaceous Ocean Climate Systems. Geol. Soc. Am., Boulder, Colorado, pp. 1–48.

Hughes, T., 1975. The West Antarctic ice sheet: instability, disintegration, and initiation of ice ages. Rev. Geophys. Space Phys. 13, 502–526.

Huybrechts, P., 1990. A 3-D model for the Antarctic ice sheet: a sensitivity study on the glacial–interglacial contrast. Clim. Dyn. 5, 79–92.

Huybrechts, P., 1990. The Antarctic ice sheet during the last glacial–interglacial cycle: a three-dimensional experiment. Ann. Glaciol. 14, 115–119.

Huybrechts, P., 1993. Glaciological modeling of the late Cenozoic East Antarctic ice sheet: stability or dynamism? Geogr. Ann. 75A, 221–238.

Huybrechts, P., 1994. Formation and disintegration of the Antarctic ice sheet. Ann. Glaciol. 20, 336–340.

Huybrechts, P., de Wolde, J., 1999. The dynamic response of the Greenland and Antarctic ice sheets to multiple century climate warming. J. Climate 1, 2169–2188.

Huybrechts, P., Oerlemans, J., 1990. Response of the Antarctic ice sheet to future greenhouse warming. Clim. Dyn. 1990, 93–102.

Lear, C.H., Elderfield, H., Wilson, P.A., 2000. Cenozoic deep-sea temperatures and global ice volumes from Mg/Ca in benthic foramineferal calcite. Science 287, 269–272.

Lenton, T.M., Cannell, M.G.R., 2002. Mitigating the rate and extent of global warming. Clim. Change 52, 255–262.

MacAyeal, D.R., 1992. Irregular oscillations of the West Antarctic ice sheet. Nature 359, 29–32.

Maqueda, M.A.M., Willmott, A.J., Bamber, J.L., Darby, M.S., 1998. An investigation of the Small Ice Cap Instability in the Southern Hemisphere with a coupled atmosphere–sea ice–ocean–terrestrial ice model. Clim. Dyn. 14, 329–352.

Mengel, J.G., Short, D.A., North, G.R., 1988. Seasonal snowline instability in an energy balance climate model. Clim. Dyn. 2, 127–131.

North, G.R., 1975. Analytical solution of a simple climate model with diffusive heat transport. J. Atmos. Sci. 32, 1301–1307.

North, G.R., 1984. The small ice cap instability in diffusive climate models. J. Atmos. Sci. 41, 3390–3395.

Oerlemans, J., 1981. Some basic experiments with a vertically integrated ice sheet model. Tellus 33, 1–11.

Oerlemans, J., 1982a. Glacial cycles and ice sheet modeling. Clim. Change 4, 353–374.

Oerlemans, J., 1982b. A model of the Antarctic ice sheet. Nature 297, 550–553.

Oerlemans, J., 2002a. On glacial inception and orography. Quat. Int. 95–96, 5–10.

Oerlemans, J., 2002b. Global dynamics of the Antarctic ice sheet. Clim. Dyn. 19, 85–93.

Oerlemans, J., 2003. A quasi-analytical ice-sheet model for climate studies. Nonlinear Process. Geophys. 10, 441–452.

Oerlemans, J., 2004. Correcting the Cenozoic $\delta^{18}O$ deep-sea temperature record for Antarctic ice volume. Palaeogeogr. Palaeoclimat. Palaeoecol. 208, 195–205.

Oerlemans, J., in press. Antarctic ice volume and deep-sea temperature during the last 50 Ma: a model study. Ann. Glaciol. 39.
Oerlemans, J., van der Veen, C.J., 1984. Ice Sheets and Climate. Reidel Publ., Dordrecht, The Netherlands, 217 pp.
Ogura, T., Abe-Ouchi, A., 2001. Influence of the Antarctic ice sheet on southern high latitude climate during the Cenozoic: albedo vs topography effect. Geophys. Res. Lett. 28, 587–590.
Pagani, M., Arthur, M.A., Freeman, K.H., 1999. Miocene evolution of atmospheric carbon dioxide. Paleoceanography 14, 273–292.
Pearson, P.N., Palmer, M.R., 2000. Atmospheric carbon dioxide over the past 60 million years. Nature 406, 695–699.
Pollard, D., 1978. An investigation of the astronomical theory of the ice ages using a simple climate–ice sheet model. Nature 272, 233–235.
Pollard, D., 1983. Ice-age simulations with a calving ice-sheet model. Quat. Res. 20, 30–48.
Pollard, D., DeConto, R.M., 2003. Antarctic climate and sediment flux in the Oligocene simulated by a climate–ice sheet–sediment model. Palaeogeogr. Palaeoclimatol. Palaeoecol. 198, 53–67.
Retallack, G.J., 2001. A 300-million-year record of atmospheric carbon dioxide from fossil plant cuticles. Nature 411, 287–290.
Retallack, G.J., 2002. Carbon dioxide and climate over the past 300 Myr. Philos. Trans. R. Soc. Lond., A 360, 659–673.
Ritz, C., Fabre, A., Letreguilly, A., 1997. Sensitivity of a Greenland ice sheet model to ice flow and ablation parameters: consequences for the evolution through the last climate cycle. Clim. Dyn. 13, 11–24.
Ritz, C., Rommelaere, V., Dumas, C., 2001. Modeling the evolution of Antarctic ice sheet over the last 420, 000 years: implications for altitude changes in the Vostok region. J. Geophys. Res. 106 (D23), 31943–31964.
Royer, D.L., Wing, S.L., Beerling, D.J., Jolley, D.W., Koch, P.L., Hickey, L.J., Berner, R.A., 2001. Paleobotanical evidence for near present-day levels of atmospheric CO_2 during part of the Tertiary. Science 292, 2310–2313.
Scherer, R.P., 1991. Quaternary and Tertiary microfossils from beneath Ice Stream B—evidence for a dynamic West Antarctic Ice Sheet history. Glob. Planet. Change 90, 395–412.
Thompson, S.L., Pollard, D., 1997. Greenland and Antarctic mass balances for present and doubled CO_2 from the GENESIS v.2 global climate model. J. Clim. 10, 871–900.
Toniazzo, T., Gregory, J.M., Huybrechts, P., 2004. Climatic impact of a Greenland deglaciation and its possible irreversibility. J. Climate 17, 21–33.
Vaughan, D.G., Spouge, J.R., 2002. Risk estimation of the collapse of the West Antarctic Ice Sheet. Clim. Change 52, 65–91.
Walker, J.C.G., Kasting, J.F., 1992. Effects of fuel and forest conservation on future levels of atmospheric carbon dioxide. Glob. Planet. Change 97, 151–189.
Warner, R.C., Budd, W.F., 1998. Modelling the long-term response of the Antarctic ice sheet to global warming. Ann. Glaciol. 27, 161–168.
Weertman, J., 1961. Stability of ice-age ice sheets. J. Geophys. Res. 66, 3783–3792.
Weertman, J., 1976. Milankovitch solar radiation variations and ice age ice sheet sizes. Nature 261, 17–20.
Zachos, J.C., Quinn, T.M., Salamy, K.A., 1996. High-resolution (10^4 years) deep-sea foraminiferal stable isotope records of the Eocene–Oligocene climate transition. Paleoceanography 11, 251–266.
Zachos, J., Pagani, M., Sloan, L., Thomas, E., Billups, K., 2001. Trends, rhythms, and aberrations in global climate 65 Ma to present. Science 292, 686–693.